JOURNAL OF SOLID STATE CHEMISTRY 62, 335–341 (1986)

Superstructure of a NASICON-Related Compound $NH_4Ti_2P_3O_{12}$

SHIGEO HORIUCHI AND AKIRA ONO

National Institute for Research in Inorganic Materials, Tsukuba, Ibaraki 305, Japan

Received May 31, 1985; in revised form September 12, 1985

Ion-pathways in a NASICON-related compound $NH_4Ti_2P_3O_{12}$ (hexagonal, $a = 0.832$ and $c = 2.34$ nm) are directly observed by means of high-resolution transmission electron microscopy. When the composition changes to $Ti_4P_6O_{23}$ due to the deammoniation as well as dehydration of heating at 770°C, a supercell with the dimensions of $A \simeq 2a$ and $C \simeq 2c$ is constructed. A model of the superstructure is proposed based on the arrangement of oxygen vacancies as well as the induced distortion of the TiO_6 octahedra, retaining the three-dimensional network in the starting structure. © 1986 Academic Press, Inc.

Introduction

$NH_4Ti_2P_3O_{12}$ is isostructural with $NaZr_2P_3O_{12}$ (*1, 2*), which is one of the end members for a series of ion-conductive NASICON compounds $Na_{1+x}Zr_2Si_xP_{3-x}O_{12}$ ($0.4 < x < 2.8$) (*3*). The structure consists of a three-dimensional network made up of PO_4 tetrahedra sharing corners with TiO_6 octahedra. NH_4^+ ions may locate at two different sites, M1 and M2, with large spaces. At room temperature, they are considered to be confined to the M1 sites. At a high temperature they must move into the M2 sites so that ion-pathways through –M2–M2– or –M2–M1–M2– become available, as have been reported for the Na^+ diffusion in the NASICON compounds (*4, 5*). Figure 1a shows a cross section of the structure. TiO_6 octahedra together with the M1 sites form the columns extending along the c axis. Figure 1b depicts a geometrical relationship between the M1 and M2 sites. Any M1 site is surrounded by six M2 sites. There are two kinds of tunnels linking the M2 sites along $[\bar{2}\bar{1}\bar{1}]$. For example, there are bottlenecks for the movement of ions along the tunnel of arrow 1 or 4, while not along the arrow 2 or 3 (*4*).

When the crystal was heated in air at the temperature 670 to 860°C, weight loss took place due to deammoniation as well as dehydration (*1*). After heating, the lattice parameters changed slightly and the chemical composition became $Ti_4P_6O_{23}$.

In the present study we have examined the structural variation during the compositional change from $NH_4Ti_2P_3O_{12}$ to $Ti_4P_6O_{23}$ on heating at 770°C, mainly by means of electron microscopy.

Experimental

$NH_4Ti_2P_3O_{12}$ was prepared at 590°C with the high-pressure vessel in the same way as reported previously (*1*). White, block crystals smaller than 0.2 mm were obtained. They show clear habit planes. The symmetry is rhombohedral ($R\bar{3}c$) according to electron diffraction and the lattice parame-

0022-4596/86 $3.00

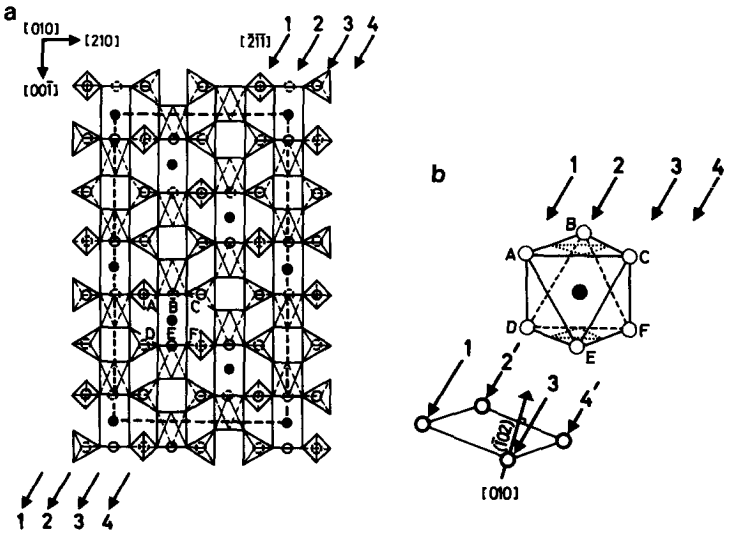

FIG. 1. Schematical representation of the crystal structure of $NH_4Ti_2P_3O_{12}$. (a) is a cross section normal to the [010] direction. TiO_6 octahedra and PO_4 tetrahedra are depicted. M1 and M2 sites are indicated by filled and open circles, respectively, c = 2.34 nm. (b) shows a three-dimensional array of the M1 and M2 sites.The triangles of dotted lines show the planes of the octahedron above or below the M1 site. The pattern of the M2 sites projected along arrows ([2$\bar{1}\bar{1}$] direction) is also shown at the bottom. Letters A to F and directions 1 to 4 are common both in (a) and (b). ($\bar{1}$02) is the plane normal to (a), including [2$\bar{1}\bar{1}$].

ters are a = 0.832 and c = 2.34 nm (for hexagonal axes) according to X-ray powder diffraction.

The crystals were then heated in air at 770°C for up to 2 hr. They were examined under an optical microscope. They were then crushed in an agate mortar and the fragments obtained were observed by a 1-MV electron microscope (H-1250 Type).

Results and Discussion

It is known that the image by modern high-resolution transmission electron microscopy (HRTEM) approximately reflects the projected potentials of crystal when taken under fixed imaging conditions (*6*). The HRTEM technique has successfully been applied to two-dimensionally ion-conductive materials like β''-alumina (*7*) and the pathways of ions were clearly visualized. For the materials with a three-dimensional network structure it is even more important to select the pertinent direction of observation. In the present case we try to observe the crystal with the incident electron beam parallel to the [2$\bar{1}\bar{1}$] direction, i.e., along the arrows in Fig. 1. Since the M2 sites are linked in lines along this direction, the projected pattern is simple as shown in Fig. 1b. The projected sites should be imaged as bright spots, when they are open or even when they are partly occupied by NH_4^+ ions.

Figure 2a is a diffraction pattern for electrons incident parallel to the [2$\bar{1}\bar{1}$] direction. It is interesting to note that the streaks appear in the direction normal to the ($\bar{1}$02) plane. Their intensity differs from one fragment to another.

The crystal is rather sensitive to electron irradiation, i.e., it rapidly changes to an amorphous state. The observation without irradiation damage is therefore limited to direct magnification lower than 10^5 times. The image in Fig. 3 was taken with the di-

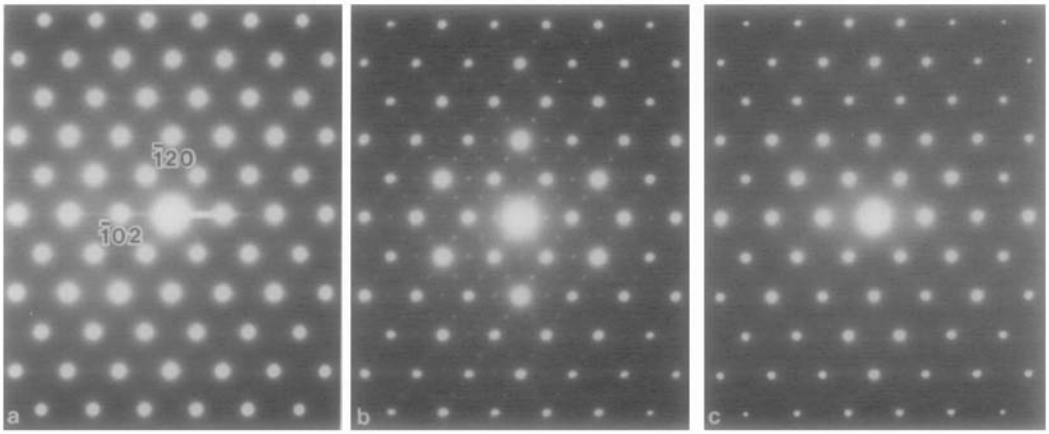

FIG. 2. Electron diffraction patterns, taken with the incident beam parallel to the $[\bar{2}\bar{1}\bar{1}]$ direction: (a) is from the starting crystal $NH_4Ti_2P_3O_{12}$; (b) and (c) are taken after the crystal was heated at 770°C. The superstructure reflexions are found in (b), but not in (c).

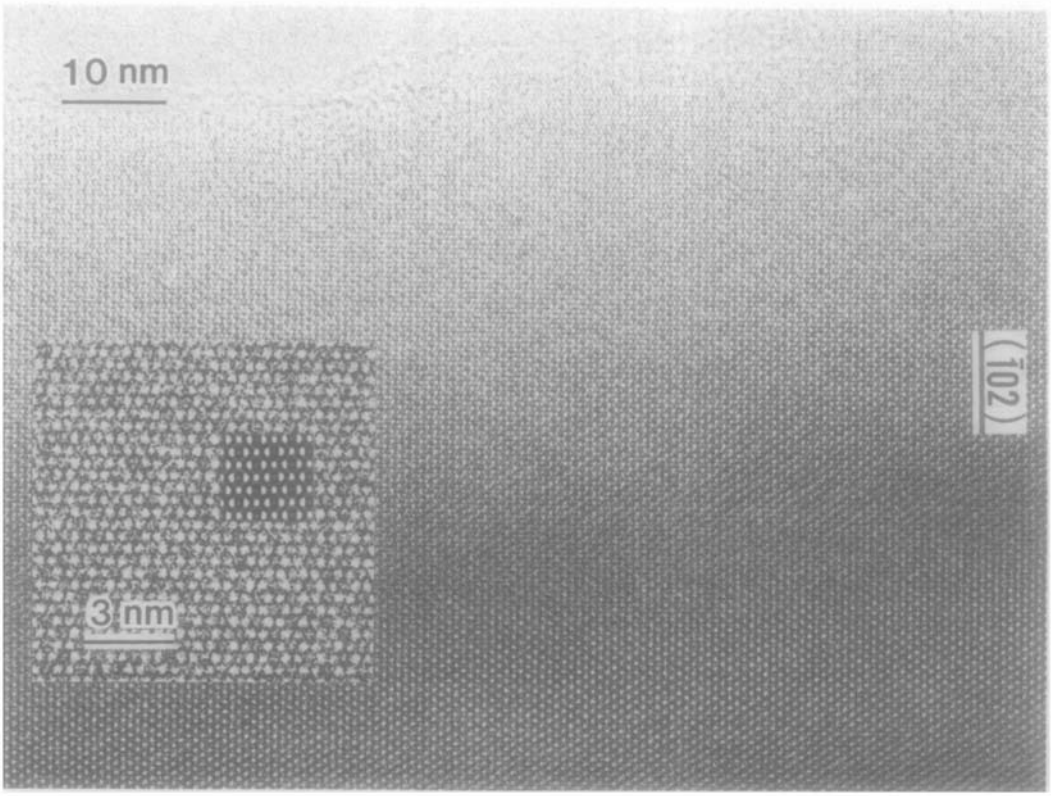

FIG. 3. A HRTEM image of $NH_4Ti_2P_3O_{12}$, corresponding to the diffraction pattern in Fig. 2a. The insert is an enlarged image of the thinnest area. In the thick area the image pattern becomes simple.

rect magnification of 7×10^4 times. The image pattern changes with the crystal thickness. The array of bright spots at the thinnest area well agrees with that expected from the projection of the M2 sites (Fig. 1b). The arrangement of network seems perfect, i.e., there are no apparent lattice defects. As we have mentioned, there are two kinds of tunnels linking the M2 sites. The image contrast of all the tunnels however, seems similar. This means that their projected potentials are almost identical.

We have calculated the image contrast using the computer simulation program, which had been reported previously (*6*). The result is represented in the enlarged part of Fig. 3, with the same magnificantion as that of the photograph. Similar images are obtained in the calculation for the crystal thinner than about 5 nm. The contrast of the real and calculated images is essentially identical. We may therefore say that the interpretation on the image contrast mentioned above is reasonable.

On heating at 770°C for 10 min, the habit planes of the crystal slightly lost the brightness under an optical microscope. The X-ray powder diffraction pattern was however almost identical with that of the crystal before heating. These observations suggest that some reactions have occurred only at the surface of crystal.

After heating the crystal for 1 hr, a number of microcracks on the habit planes were observed under an optical microscope. On the X-ray powder diffractometer chart, the positions of reflexions were similar to those of $NH_4Ti_2P_3O_{12}$, although all the peaks strongly reduced the intensity with high background scattering. The lattice parameters obtained from the chart are $a' = 0.838$ nm and $c' = 2.21$ nm. These values almost coincide with those reported for $Ti_4P_6O_{23}$ (*1*).

On the electron diffraction patterns, the streaks normal to $(\bar{1}02)$ disappeared and, instead, for the majority of the fragments weak spots appeared at the middle points between the spots from $NH_4Ti_2P_3O_{12}$ (Fig. 2b). This indicates that the structure of $Ti_4P_6O_{23}$ is formed by a supercell of that of $NH_4Ti_2P_3O_{12}$. From a series of diffraction patterns the size of the supercell is determined to be $A = 2a'$ and $C = 2c'$.

The image corresponding to Fig. 2b is shown in Fig. 4. The crystal seems to be composed of small domain-like areas, which are mutually misoriented. The arrangement of bright spots at some local areas marked by arrows is similar to that at the lower, thick part of Fig. 3. The image pattern smoothly changes from the area to the surrounding. The image calculated for $NH_4Ti_2P_3O_{12}$ with the incident electrons parallel to $[\bar{2}\bar{1}\bar{1}]$ coincides well with that of the area indicated by arrows. Similar simulation images are obtained for the crystal with thickness between 8 and 15 nm. When the incident electrons deviate from $[\bar{2}\bar{1}\bar{1}]$, the calculated images change so as to decrease the symmetry in the pattern, as observed in Fig. 4.

The above observation relating to Fig. 4 together with the finding through the electron diffraction in Fig. 2b indicates that the superlattice is constructed while keeping the structural network in $NH_4Ti_2P_3O_{12}$. In considering the composition $Ti_4P_6O_{23}$, oxygen vacancies must be included in the network. Their regular arrangement may induce the superstructure.

The following model of the superstructure can then be proposed; sites A to F in Fig. 5a are relatively far from the open spaces M1 and M2. Oxygen vacancies will appear at one of these sites preferentially. The formation of a vacancy necessarily induces the distortion of the related octahedron. For example, if a vacancy is tentatively formed at the site A, the oxygen at the site B must slightly shift in the direction indicated by the arrow. An oxygen at C as well as other surrounding atoms, including a cation at the center of the octahedron,

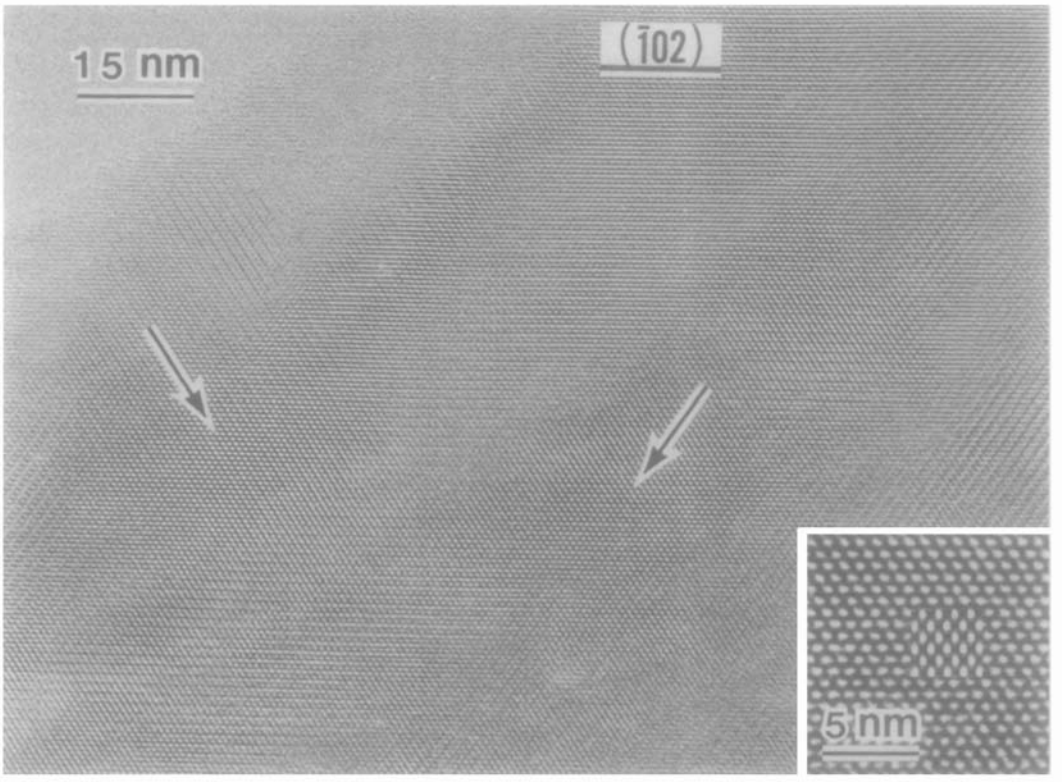

FIG. 4. Electron micrograph of the superstructure, which gives the diffraction pattern in Fig. 2b. The insert at the lower right is enlarged from the areas indicated by arrows.

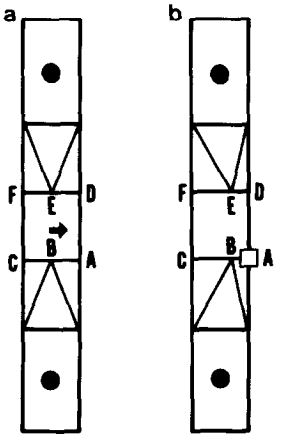

FIG. 5. (a) A column of TiO_6 octahedra showing the possible sites of vacancies. (b) Schematic representation of the distortion of octahedra caused by the formation of a vacancy (square).

must also move. However, we neglect the movement except that of the oxygen at B, for simplicity. We depict such atomic movement as in Fig. 5b. In the octahedron at the opposite site the distortion must be as schematically shown in the figure; since the triangular planes facing each other tend to be in a like orientation so that the open space between them will be as small as possible in volume.

It is estimated from the composition $Ti_4P_6O_{23}$ that, on an average, one oxygen vacancy is included in a column of octahedra with the length of the conventional unit cell along the c axis (see Fig. 1a). The probability of forming a vacancy at any site among A to F is identical. As a special case, however, we may expect that two (A and C) of these sites are tentatively selected and

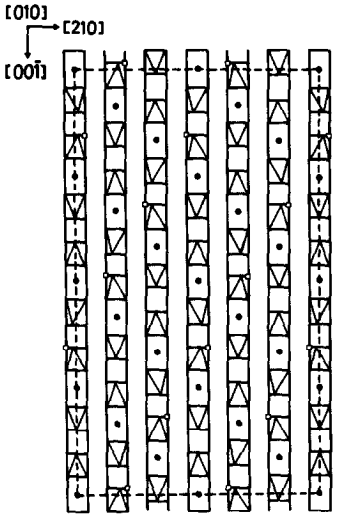

FIG. 6. A model for the superstructure, $c = 4.42$ nm. Squares mean oxygen vacancies. The distortion of TiO_6 octahedra are schematically shown. PO_4 tetrahedra are abbreviated for simplicity.

arrayed as depicted in Fig. 6, where the superlattice is formed with twice the periodicity in the c direction as well as in the lateral direction. It is noted in Fig. 6 that the sites of the vacancies are as far apart as possible to each other so that the strain around each vacancy is minimized.

In reality, vacancies at the site other than the two chosen above are possible since their formation does not increase the strain energy much. The real superstructure must therefore be highly incomplete and definite pairs of vacancy sites are selected only in small limited regions. This may be the reason why the superlattice is composed of small domain-like areas in the HRTEM images.

The present superstructure is characteristic in that it is formed at high temperature. Irregularity in the arrangement of vacancy sites must contribute to enhancing the configurational entropy.

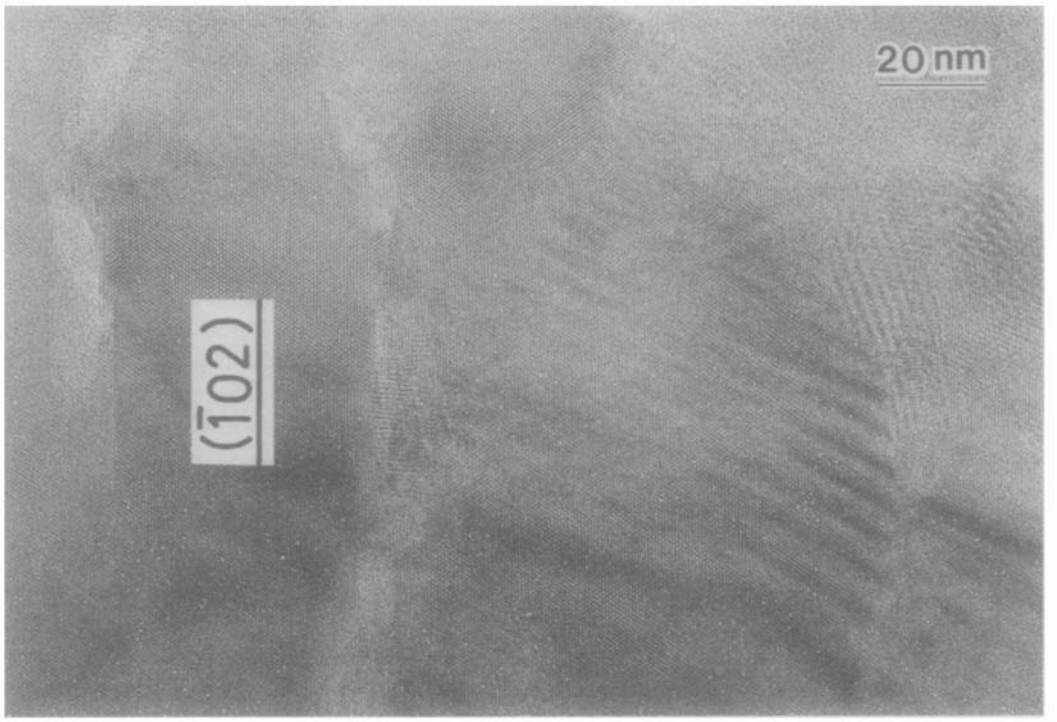

FIG. 7. Electron micrograph of the area where the superstructure is not formed in spite of heating.

For a minor group of the fragments heated for 1 hr, we have found neither extra spots nor diffuse streaks in the diffraction pattern (Fig. 2c). The fragments were often divided into band-like regions (Fig. 7). Most of the bands are definitely oriented; in the case of Fig. 7, the wall of the bands is nearly parallel to the $(\bar{1}02)$ plane. In each band, the image patterns are apparently varied from area to area. It is considered from the morphology that the microcracks observed under an optical microscope have occurred near the area. The reason why the superstructure is not formed in these areas seems to be related to the fact that they are severely distorted.

In Fig. 2c there are no diffraction streaks. The formation of the streaks in Fig. 2a is therefore related to the fact that NH_4^+ ions are included in the crystal. A possible explanation for the origin of the streaks may be that the NH_4^+ ions partly move out from the M1 sites even at room temperature and irregularly distribute at the M2 sites. The large fluctuation in the $(\bar{1}02)$ lattice spacing is induced to cause the diffraction streaks.

On increasing the heating period to 2 hr main reflexions on the X-ray diffractometer chart were identified as TiP_2O_7 and $Ti_5P_4O_{20}$ with a slight amount of $Ti_4P_6O_{23}$ (*1*). Electron diffraction patterns also showed that the superstructure mentioned above still remained slightly.

For comparison, we have examined the structural change in $NH_4Zr_2P_3O_{12}$. At the first stage of heating $HZr_2P_3O_{12}$ were formed by deammoniation and, simultaneously, the crystal was separated into small particles of a few hundred nanometers, in accordance with the previous report (*8*). At the second stage, dehydration has occurred to change the composition to $Zr_4P_6O_{23}$ but no superlattice has been found in the particles. The reason for no existence of superlattice must owe to the fact that the particles are very small, because the regular arrangement of oxygen vacancies in Fig. 6 is difficult at or near the surface of the crystal.

References

1. A. Ono, *J. Solid State Chem.* **56,** 260 (1985).
2. L. Hagman and P. Kierkegaard, *Acta Chem. Scand.* **22,** 1822 (1968).
3. H. Y.-P. Hong, *Mater. Res. Bull.* **11,** 173 (1976).
4. D. Tran Qui, J. J. Capponi, J. C. Joubert, and R. D. Shannon, *J. Solid State Chem.* **39,** 219 (1981).
5. H. Kohler, H. Schulz, and O. Melinikov, *Mater. Res. Bull.* **18,** 1143 (1983).
6. S. Horiuchi, *Ultramicroscopy* **10,** 229 (1982).
7. Y. Matsui and S. Horiuchi, *Acta Crystallogr. Sect. A* **37,** 51 (1981).
8. A. Ono, *J. Mater. Sci.* **19,** 2691 (1984).